UC Santa Cruz
UC Santa Cruz Previously Published Works

Title

NHR-23 and SPE-44 regulate distinct sets of genes during Caenorhabditis elegans spermatogenesis

Permalink

https://escholarship.org/uc/item/2560s77m

Journal

G3: Genes, Genomes, Genetics, 12(11)

ISSN

2160-1836

Authors

Ragle, James Matthew
Morrison, Kayleigh N
Vo, An A
et al.

Publication Date

2022-11-04

DOI

10.1093/g3journal/jkac256

Peer reviewed

NHR-23 and SPE-44 regulate distinct sets of genes during *Caenorhabditis elegans* spermatogenesis

James Matthew Ragle [ID] ,[1] Kayleigh N. Morrison [ID] ,[2] An A. Vo [ID] ,[1] Zoe E. Johnson [ID] ,[1] Javier Hernandez Lopez [ID] ,[1] Andreas Rechtsteiner [ID] ,[1] Diane C. Shakes [ID] ,[2,]* Jordan D. Ward [ID] [1,]*

[1]Department of Molecular, Cell, and Developmental Biology, University of California, Santa Cruz, CA 95064, USA
[2]Department of Biology, William & Mary, Williamsburg, VA 23185, USA

*Corresponding author: Department of Molecular, Cell, and Developmental Biology, University of California, Santa Cruz, CA 95064, USA.
Email: jward2@ucsc.edu; *Corresponding author: Department of Biology, William & Mary, Williamsburg, VA 23185, USA. Email: dcshak@wm.edu

Abstract

Spermatogenesis is the process through which mature male gametes are formed and is necessary for the transmission of genetic information. While much work has established how sperm fate is promoted and maintained, less is known about how the sperm morphogenesis program is executed. We previously identified a novel role for the nuclear hormone receptor transcription factor, NHR-23, in promoting *Caenorhabditis elegans* spermatogenesis. The depletion of NHR-23 along with SPE-44, another transcription factor that promotes spermatogenesis, caused additive phenotypes. Through RNA-seq, we determined that NHR-23 and SPE-44 regulate distinct sets of genes. The depletion of both NHR-23 and SPE-44 produced yet another set of differentially regulated genes. NHR-23-regulated genes are enriched in phosphatases, consistent with the switch from genome quiescence to post-translational regulation in spermatids. In the parasitic nematode *Ascaris suum*, MFP1 and MFP2 control the polymerization of Major Sperm Protein, the molecule that drives sperm motility and serves as a signal to promote ovulation. NHR-23 and SPE-44 regulate several MFP2 paralogs, and NHR-23 depletion from the male germline caused defective localization of MSD/MFP1 and NSPH-2/MFP2. Although NHR-23 and SPE-44 do not transcriptionally regulate the casein kinase gene *spe-6*, a key regulator of sperm development, SPE-6 protein is lost following NHR-23+SPE-44 depletion. Together, these experiments provide the first mechanistic insight into how NHR-23 promotes spermatogenesis and an entry point to understanding the synthetic genetic interaction between *nhr-23* and *spe-44*.

Keywords: *Caenorhabditis elegans*; spermatogenesis; NHR-23; SPE-44; nuclear hormone receptor; transcription factor; gene regulation

Introduction

Spermatogenesis involves a cascade of morphogenetic events to produce the highly specialized, haploid, motile gametes essential for sexual reproduction (Fabian and Brill 2012; Ellis and Stanfield 2014; Nishimura and L'Hernault 2017). Universal features of spermatogenesis include the biosynthesis of sperm-specific proteins and assembly of sperm-specific complexes, preparing for and progressing through the meiotic divisions, and a streamlining step during which cells discard cytoplasmic components that are no longer needed (Nishimura and L'Hernault 2017). At species-specific points during sperm development, transcription ceases; the final steps of differentiation and mature sperm function occur in the absence of transcription (D'Occhio *et al.* 2007; Rathke *et al.* 2007; Shakes *et al.* 2009). The sperm's genome is protected from environmental and metabolic damage through a spermatogenesis-specific process of chromatin remodeling and hypercompaction (Wu and Chu 2008). These processes are all essential for the faithful transmission of the sperm genome to offspring.

Caenorhabditis elegans is a powerful model to study spermatogenesis. Within the self-fertile hermaphrodites, uncommitted germ cells have the capacity to undergo either spermatogenesis or oogenesis; but in the normal process, the hermaphroditic germline makes a one-time switch from spermatogenesis to oogenesis as animals enter adulthood. The analysis of the accompanying changes provides insight into how sperm and egg fates are promoted and maintained. Alternatively, the analysis of males allows the study of continual spermatogenesis. Both hermaphrodite and male germlines are polarized organs; the uncommitted germ cells proliferate mitotically at the distal end before committing to entering the meiotic prophase and commitment to the sperm fate. The events of meiosis occur in a linear fashion along the length of the gonad, resulting in the production of haploid spermatids. These include homologous chromosome pairing, DNA breaks that promote recombination, and 2 meiotic divisions (Shakes *et al.* 2009; Chu and Shakes 2013; Ellis and Stanfield 2014; Griswold 2016). During *C. elegans* spermatogenesis, general transcription ceases near the end of the meiotic prophase, and there is no burst of postmeiotic transcription as occurs in humans and *Drosophila* (Bettegowda and Wilkinson 2010; Chu and Shakes 2013). The translation ceases shortly after anaphase II, as not only ribosomes but also tubulin, actin, and endoplasmic reticulum are partitioned away from the budding spermatids and into a structure known as the residual body (Chu
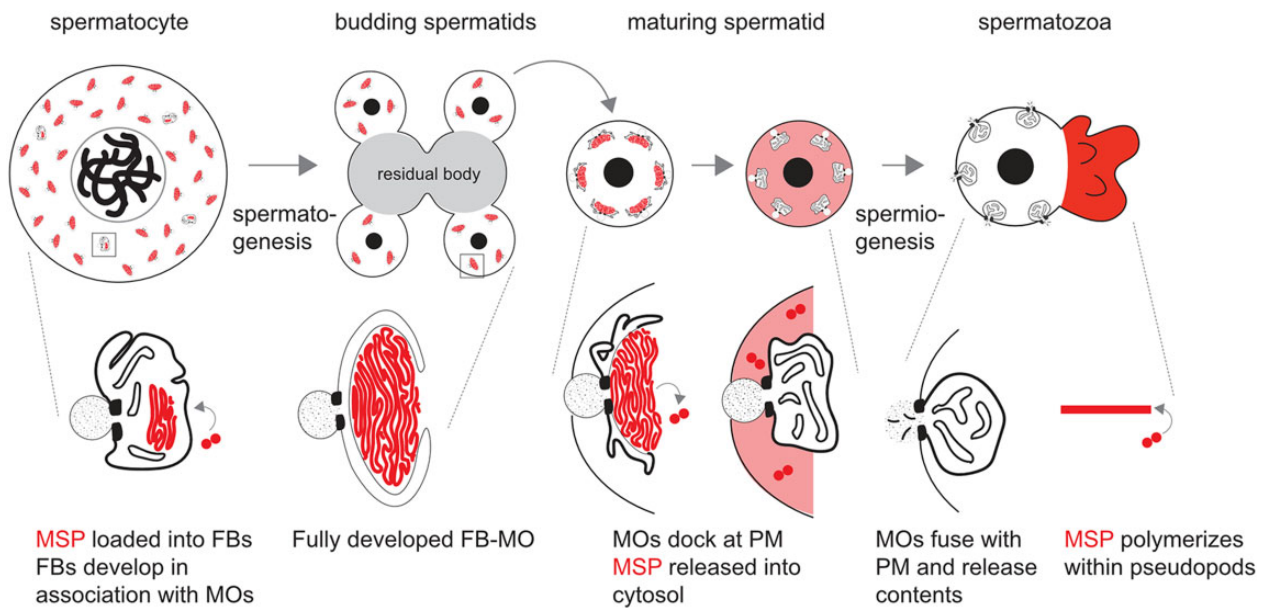
Fig. 1. Overview of MSP dynamics during spermatogenesis. (Top) Spermatocytes undergo reductive cell division during spermatogenesis. During this process, MSP is packaged and sequestered in FB-MOs. Following anaphase II, components which are no longer needed partition to central residual bodies, which are discarded. Spermatids bud off of the residual bodies, mature, and upon activation, undergo morphological changes during spermiogenesis. The differentiated spermatozoa contain cell bodies and pseudopodia. (Bottom) Within spermatocytes, FBs develop on the cytosolic face of the Golgi-derived MO. During the budding division, FB-MO complexes partition to the spermatids. In maturing spermatids, MOs dock with the plasma membrane as the FBs disassemble and release MSP dimers into the cytosol. During sperm activation, MSP localizes to the pseudopod, where it polymerizes, and MOs fuse with the plasma membrane.

and Shakes 2013; Fig. 1). Lacking typical cytoskeletal proteins, nematode sperm motility is driven by the assembly/disassembly dynamics of the 14 kDa nematode-specific major sperm protein (MSP) within the pseudopod of the crawling spermatozoa (Smith 2014). The early cessation of both transcription and translation requires all sperm-specific components to be synthesized during meiotic prophase prior to their developmental deployment. During this critical window, newly synthesized MSP assembles into large paracrystalline fibrous bodies (FBs) that form in association with Golgi-derived membranous organelles (MOs; Fig. 1). This form of MSP packaging facilitates the efficient partitioning of MSP to spermatids.

The transcription and translational programs that govern *C. elegans* spermatogenesis must not only drive differentiation of spermatocytes and oocytes, but they must also create the materials that are needed for sperm differentiation and sperm function. How early-acting gene regulatory networks provision spermatocytes for the extended process of spermatogenesis and sperm morphogenesis remains an open question. To date, 2 transcription factors have been characterized as critical regulators of *C. elegans* spermatogenesis: SPE-44 and NHR-23. SPE-44 was first identified by its enrichment in sperm-producing germlines. Further investigation revealed that *spe-44* null spermatocytes fail to load MSP into FB-MOs, and they are arrested as terminal spermatocytes during the second meiotic division (Kulkarni *et al.* 2012). *spe-44* regulates a broad set of genes that are enriched in spermatogenic germlines (Kulkarni *et al.* 2012). Consistent with the MSP loading defects, these genes include MSP genes and members of the small sperm-specific protein family, which promote MSP polymerization (Kulkarni *et al.* 2012). *spe-44* also regulates several genes necessary for spermatogenesis, which were previously identified through forward genetic screens for spermatogenesis defective (*spe*) and fertilization-defective (*fer*) genes (Kulkarni *et al.* 2012). However, many other *spe* and *fer* genes are

not regulated by *spe-44* (Kulkarni *et al.* 2012). In terms of regulatory hierarchies, *spe-44* regulates the transcription factor, *elt-1* (Kulkarni *et al.* 2012), which is a direct regulator of MSP gene expression (del Castillo-Olivares *et al.* 2009).

We recently discovered that the nuclear hormone receptor NHR-23, a critical regulator of nematode molting, is also expressed in primary spermatocytes and necessary for spermatogenesis (Ragle *et al.* 2020). NHR-23 and SPE-44 expression patterns almost completely overlap (Ragle *et al.* 2020). Both proteins label the autosomes but not the X-chromosome from the beginning of the meiotic prophase until global transcription ceases and spermatocytes enter the karyosome stage. Germline-specific NHR-23 depletion causes a terminal spermatocyte arrest during the first meiotic division (Ragle *et al.* 2020). Spermatocytes fail to load MSP into FBs upon single depletion of either SPE-44 or NHR-23, whereas the Golgi-derived MO portion of the FB-MO complex is specifically perturbed upon SPE-44 depletion and severely disrupted upon double depletion (Ragle *et al.* 2020). We determined that SPE-44 and NHR-23 are in separate genetic pathways because they do not regulate one another, and because NHR-23 and SPE-44 double depletion produce more severe synthetic phenotypes such as a nearly complete loss of MO differentiation markers and severe germline defects (Ragle *et al.* 2020). Exactly how NHR-23 promotes spermatogenesis was not clear from our previous work. Here, we use a combination of transcriptomics, genome editing, and cytology to address this question and gain insight into the synthetic genetic interaction between *spe-44* and *nhr-23*.

Materials and methods
Strains and culture

Caenorhabditis elegans were cultured as originally described (Brenner 1974), except that worms were grown on MYOB media

instead of NGM. MYOB agar was made as previously described (Church *et al.* 1995). Brood sizes were performed picking L4 larvae to individual wells of a 6-well plate seeded with OP50 and incubating the plate at 20°C. Animals were transferred to new plates daily over 4 days. Two days post-transfer, the number of hatched progeny and unfertilized eggs were scored. We scored unfertilized eggs over the first 3 days as on the fourth day animals frequently ran out of sperm.

Table 1 contains a list of all the strains used and their source.

RNA-seq and bioinformatics

Adult hermaphrodites of the indicated genotypes were picked onto 6 cm MYOB + 4 mM auxin plates and allowed to lay eggs for 2 h. The hermaphrodites were removed, and the plates were incubated at 20°C for 3 days. All strains carried an *him-5 (e1490)* allele to increase the number of males in hermaphrodite progeny. Five hundred L4/young adult males were hand-picked into M9 + 0.05% gelatin, washed 1X, and pelleted. Liquid was removed down to 25 µl and 500 µl TRIzol (Invitrogen) was added. The mixture was incubated at room temperature for 5 min with periodic vortexing. Carcasses were pelleted by centrifugation and the supernatant was removed to a clean tube. One hundred microliters chloroform was added to the supernatant, vortexed for 30 s and phases separated by centrifugation at 15,000 RPM for 5 min. Two hundred and fifty microliters of the upper aqueous phase was removed to a new tube and 350 µl chloroform was added, vortexed, and separated as in the previous steps. Two hundred and fifty microliters of isopropanol was added to the aqueous phase along with 1 µl Glycoblue (Invitrogen) and vortexed. The solution was centrifuged for 20 min at 15,000 RPM and the supernatant was decanted. The pellet was washed with 1 ml 75% ethanol twice and dried at room temperature for 10 min. The dried pellet was resuspended in 16 µl nuclease-free water. The RNA concentration was determined with a NanoDrop.

Using the NEXTFLEX Rapid Directional RNA-Seq Kit 2.0 (BioO/PerkinElmer), polyA-selected RNA was isolated from 300 ng of total RNA according to the manufacturer's instructions. The sequencing libraries were prepared using the same kit according to manufacturer's instructions. The concentrations were measured on a Qubit Fluorometer (Invitrogen) and fragment size

determined on a Bioanalyzer 2100 (Agilent). Libraries were sequenced at the University of California Berkeley QB3 NGS facility on a Nova-seq platform. Raw sequences were mapped to transcriptome version WS220 using Tophat2 (Kim *et al.* 2013). Only reads with one unique mapping were retained, otherwise, default options for paired-end mapping were used. HTSeq was used to obtain read counts per transcript (Anders *et al.* 2015). All libraries were sequenced twice and for each transcript read counts from both sequencing runs were added together. DESeq2 was used for read count normalization and differential expression analysis (Love *et al.* 2014). DESeq2's regularized log transformation with option blind=TRUE was used for read count normalization of protein-coding genes prior to principal component analysis (PCA). A Benjamini–Hochberg multiple hypothesis-corrected P-value cutoff of 0.05 was used as a cutoff for significant differential expression. PCA was performed using the prcomp function in the stats package of R (R Core Team). Supplementary Table 1 contains the processed data with gene name and location, mean expression, log2 fold-change compared to control, and P-value. The 3D PCA scatter plot was generated with http://www.bioinformatics.com.cn/srplot (last accessed Sept. 27, 2022), an online platform for data analysis and visualization. Protein and cDNA alignments were produced with Clustal Omega (Goujon *et al.* 2010; Sievers *et al.* 2011). Protein alignments were visualized with JalView2 (Waterhouse *et al.* 2009). Venn diagrams were generated using GeneVenn (http://genevenn.sourceforge.net/; last accessed Sept. 27, 2022) and figures were generated in Affinity Designer.

CRISPR/Cas9-mediated genome editing

The mutations in candidate NHR-23 target genes were generated using homologous recombination of CRISPR/Cas9-induced double-strand breaks (DSBs). We made Cas9 ribonucleoprotein (RNP) complexes (750 ng/µl house-purified Cas9, 50 ng/µl crRNA, and 100 ng/µl tracrRNA) by incubating at 37°C for 15 min. RNPs were mixed with oligonucleotide repair templates (110 ng/µl; Ghanta and Mello, 2020; Paix *et al.* 2015; Dokshin *et al.* 2018) and a coinjection marker (either 50 ng/µl pRF4, 1–10 ng/µl pKA411, or 25 ng/µl pSEM229; El Mouridi *et al.* 2020) to facilitate isolation of successfully injected progeny. Where possible, we selected "GGNGG" crRNA targets as these have been the most robust in our hand

Table 1. List of strains used.

Strain	Genotype	Source/reference
N2	Wild type	CGC
JDW85	*wrdSi14[mex-5p::TIR1: F2A: mTagBFP2: tbb-2 3'UTR, I:-5.32]; him-5(e1490) V.*	Ragle *et al.* (2020)
JDW86	*wrdSi15[mex-5p::TIR1: F2A: mTagBFP2: tbb-2 3'UTR, I:-5.32]; spe-44(fx110[spe-44::AID*]) IV; him-5(e1490) V.*	Ragle *et al.* (2020)
JDW92	*wrdSi19[mex-5p::TIR1: F2A: mTagBFP2: tbb-2 3'UTR, I:-5.32], nhr-23(kry61(nhr-23::AID*-TEV-3xFLAG)) I; him-5(e1490) V.*	Ragle *et al.* (2020)
JDW146	*wrdSi19[mex-5p::TIR1: F2A: mTagBFP2: tbb-2 3'UTR, I:-5.32], nhr-23(kry61(nhr-23::AID*-TEV-3xFLAG)) I; spe-44(fx110[spe-44::degron]) IV; him-5(e1490) V.*	Ragle *et al.* (2020)
JDW307	*nsph-3.2(wrd56[C04G2.9::exon 1 STOP]) IV*	This study
JDW308	*nsph-2(wrd57[ZK265.3::exon 1 STOP]) I*	This study
JDW320	*nsph-2(wrd57[ZK265.3::exon 1 STOP]) I; nsph-3.2(wrd56[C04G2.9::exon 1 STOP]) IV*	This study
JDW339	*nsph-2(wrd57[ZK265.3::exon 1 STOP]) I; nsph-1.1(wrd67[K08F8.5::exon 2 STOP]) II*	This study
JDW358	*ZK596.2(wrd71[exon 1 STOP]) III*	This study
JDW361	*ttbk-5(wrd72[exon 1 STOP]) IV*	This study
JDW367	*nsph-4.3(wrd74[T04A6.4 exon 1 STOP]) III*	This study
JDW374	*ZK757.2(wrd77[exon-1 STOP]) III*	This study
JDW403	*nsph-4.1(wrd92[whole gene deletion]) IV*	This study
JDW404	*nsph-4.2(wrd93[whole gene deletion]) IV*	This study
JDW427	*nsph-4.1(wrd92[whole gene deletion]), nsph-4.2(wrd97[whole gene deletion]) IV*	This study
RV120	*spe-44(ok1400) dpy-20 (e1282)/let-92 (s677) unc-22 (s7) IV ok1400 deletion removes 1,577 of the 1,797 base-pair coding region, including the conserved SAND domain. Presumed null*	Kulkarni *et al.* (2012)

and support efficient editing (Farboud and Meyer 2015). All STOP-IN cassettes were designed to be inserted directly at the DNA DSB site. Sequences and descriptions of the crRNAs and repair oligos are provided in Supplementary Tables 2 and 3, respectively. We picked L4 animals, aged them 1 day at 20°C and injected 6–18 animals for each edit. Injected animals were grown at either 20°C or 25°C until progeny were produced. These progenies were isolated to individual plates to lay eggs. We made genomic lysates from parent animals and genotyped them by polymerase chain reaction using primers that anneal to sites flanking the mutations. As our version of the STOP-IN cassette contains a *Bam*HI site, insertions were identified by diagnostic *Bam*HI digestion. Whole gene deletions were identified by PCR product size. Mutations and homozygosity were verified by Sanger sequencing. Genotyping primers are provided in Supplementary Table 4. Knock-in sequences are provided in Supplementary File 1.

Immunocytochemistry

Embryos were isolated from adult hermaphrodites of the indicated genotypes by standard bleaching methods (dx.doi.org/10.17504/protocols.io.j8nlkkyxdl5r/v1; last accessed Sept. 27, 2022) and allowed to hatch overnight in the absence of food. L1 larvae were transferred to multiple OP50 plates for 6–8 h. The treatment groups were washed off the plates and transferred to MYOB + 4 mM auxin plates. Sibling controls were kept on non-auxin plates. Both groups were raised to adulthood at room temperature. Sperm spreads were obtained by dissecting 10–12 male worms in 7 µl of egg buffer (Edgar 1995) on ColorFrost Plus slides (Fisher Scientific, 12-550) that were additionally coated with poly-L-lysine (Sigma Aldrich, P8290). Worms of different genotypes were dissected on the same slide to ensure that antibody binding conditions were competitive and identical. During analysis, mutants were distinguished by their DAPI-stained nuclear patterns. Separate immunocytology preps were performed with worms of different genotypes on different slides to help identify the phenotypes observed on mixed slides. Samples were freeze-cracked in liquid nitrogen and fixed overnight in −20°C methanol. Specimen preparation and antibody labeling followed established protocols (Shakes *et al.* 2009). Primary antibodies included: 1:300 rabbit anti-MSD-1 (F44D1.3) polyclonal (Kosinski *et al.* 2005), 1:200 rabbit anti-MFP2/NSPH-2 (ZK265.3) polyclonal (Morrison *et al.* 2021), and 1:250 rabbit anti-SPE-6 (Peterson *et al.* 2021). 1:400 Alexa Fluor Plus 555 goat anti-rabbit IgG (Invitrogen, A32732) was used as the secondary antibody. Final slides were mounted with Fluoro Gel with DABCO (Electron Microscopy Sciences #17985-02) containing DAPI. Images were acquired with epifluorescence using an Olympus BX60 microscope equipped with a QImaging EXi Aqua CCD camera. Photos were taken, merged, and exported for analysis using the program iVision. Image exposures were optimized for control samples and then all samples were imaged with the same exposures and no further image processing so that images would reflect relative intensities.

Results

NHR-23 and SPE-44 regulate distinct sets of target genes

Given that NHR-23 is a transcription factor, we hypothesized that loss of NHR-23-regulated gene expression was mediating the phenotypes we observed when NHR-23 was depleted. We therefore depleted NHR-23, SPE-44, and NHR-23+SPE-44 in male germlines using a *mex-5p::TIR1* transgene that we developed for an auxin-inducible degron toolkit (Ashley *et al.* 2021). We performed bulk RNA-seq on whole male animals to identify differentially regulated genes relative to a *mex-5p::TIR1* control strain grown on auxin. With our sequencing data, we performed PCA of the replicates of all conditions. The first 3 principal components captured 63% of the variance and separated the various conditions (Fig. 2, a and b, Supplementary Fig. 1). Using a $P < 0.05$ cutoff, there were only 70 genes that significantly changed in expression when NHR-23 was depleted (Fig. 2c, Supplementary Table 5). NHR-23 appeared to function primarily to activate gene expression as 55/70 genes were downregulated following NHR-23-depletion (Fig. 2c). SPE-44-depletion resulted in 811 differentially expressed genes, with 523 genes being downregulated (Fig. 2d, Supplementary Table 6). For all 3 datasets, we set the cutoff for differentially regulated genes as a >1.5-fold change in expression relative to the control. NHR-23+SPE-44 double depletion produced 554 differentially expressed genes, with 494 being downregulated (Fig. 2e, Supplementary Table 7). When compared with an RNA-seq study of spermatogenesis vs oogenesis enriched genes (Ortiz *et al.* 2014), NHR-23-regulated and NHR-23+SPE-44-regulated genes had a high percentage [72.9% (51/70) and 84.3% (467/554), respectively] of sperm-enriched genes (Fig. 2, g and h). In contrast, only 59.9% (306/511) of SPE-44-regulated genes were spermatogenesis-enriched (Fig. 2i). A *spe-44* mutant microarray experiment found 50.9% (358/703) genes were spermatogenesis-enriched, though this percentage went to 67.8% (343/506) if only the downregulated genes were analyzed (Kulkarni *et al.* 2012). When we performed a similar analysis on our SPE-44-downregulated genes we found 53.5% (296/553) were spermatogenesis-enriched (Supplementary Fig. 2a).

We were surprised to find so few differentially regulated genes following NHR-23 depletion in the germline as *nhr-23* regulates 265 genes in the soma (Kouns *et al.* 2011). NHR-23 regulated genes included a few genes previously implicated in spermatogenesis. NHR-23 regulated the MSP Domain containing proteins MSD-1, MSD-2, and MSD-3 which are poorly characterized paralogs of *Ascaris* MSP fiber protein 1 (MFP1), an MSP polymerization inhibitor (Buttery *et al.* 2003; Grant *et al.* 2005; Kosinski *et al.* 2005; Morrison *et al.* 2021; Table 2). *smz-2* was also NHR-23 regulated (Table 2). *smz-2* has a paralog (*smz-1*), and the proteins SMZ-1/2 localize to chromatin during meiosis (Chu *et al.* 2006). In addition, RNAi targeting of either SMZ gene causes a metaphase arrest during meiosis (Chu *et al.* 2006). In contrast to the short list of NHR-23-regulated genes, we found 811 genes that were differentially expressed upon SPE-44 depletion (Fig. 2, Supplementary Table 6) and 554 genes differentially expressed when both NHR-23 and SPE-44 were depleted (Fig. 2, Supplementary Table 7). Surprisingly, our SPE-44-regulated gene set had limited overlap with a set of *spe-44*-regulated genes identified through a microarray experiment using *spe-44* null L4 males (Kulkarni *et al.* 2012). Only 180 of the 811 SPE-44-regulated genes from our RNA-seq dataset were common to the *spe-44* null microarray dataset (Supplementary Fig. 2b). This discrepancy may be due to SPE-44 depletion causing a reduction-of-function while the mutant is a null (Kulkarni *et al.* 2012). The transcription factor *elt-1*, a downstream target of *spe-44*, was found in both the microarray and RNA-seq datasets, as was *spe-18*, which was validated by promoter reporters in Kulkarni *et al.* (2012; *spe-18* referred to as *spe-7* in that paper; Table 2). Two *msp* genes (*msp-49*, *msp-63*) were common to the microarray and RNA-seq datasets (Table 2). There were 5 *spe* genes that were downregulated in our RNA-seq data, but not in the *spe-44* microarray (Table 2). Three genes encode membrane proteins required for fertilization (*spe-9*, *spe-42*, *spe-49*), *spe-43* is required for sperm activation, and *spe-45* is required
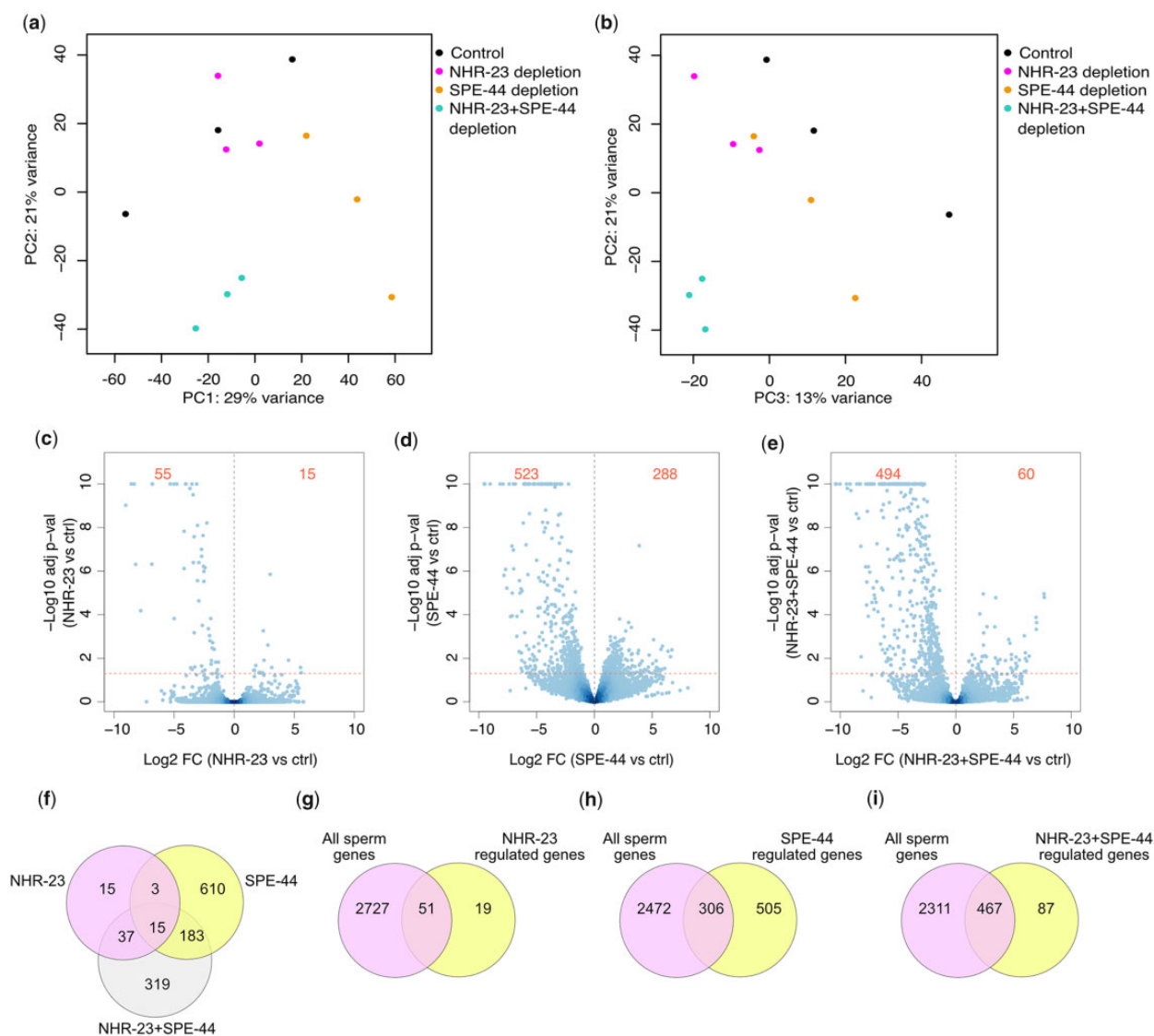
Fig. 2. NHR-23 and SPE-44 regulate distinct sets of genes. a and b) PCA of RNA-seq data. Legend indicates which data points belong to control, NHR-23-depleted, SPE-44-depleted, or NHR-23+SPE-44-depleted biological replicates. c–e) Volcano plots of the indicated depletion datasets showing Log10 adjusted *P*-value against Log2 fold-change (FC). The horizontal dotted line represents our *P*-value cutoff of 0.05 and the vertical dotted line indicates a fold-change of 0. The red numbers in each figure indicate the number of differentially downregulated (left side) and upregulated (right side) genes in each comparison with a fold-change cutoff >1.5 (log2 = 0.58) and *P* < 0.05. f) Venn diagram depicting overlap of differentially regulated genes following NHR-23-, SPE-44, and NHR-23+SPE-44 depletion. Venn diagrams depicting overlap between sperm-enriched genes (Ortiz *et al.* 2014) and differentially regulated genes following NHR-23 depletion (g), SPE-44-depletion (h), and NHR-23+SPE-44 depletion (i).

for sperm to fuse with the oocyte plasma membrane (Singson *et al.* 1998; Zannoni *et al.* 2003; Kroft *et al.* 2005; Nishimura *et al.* 2015; Krauchunas *et al.* 2018; Wilson *et al.* 2018; Takayama *et al.* 2021). While our current focus in this study is on how NHR-23 promotes spermatogenesis, exploring the commonalities and differences between our RNA-seq data and the microarray data is an important future direction to further elucidate how SPE-44 promotes sperm development.

There were 326 differentially regulated genes unique to NHR-23+SPE-44-depleted males, consistent with the additive phenotype when we deplete both SPE-44 and NHR-23 (Ragle *et al.* 2020; Fig. 2). These genes included 14 *msp* genes, as well as *smz-1*, the paralog of NHR-23-regulated *smz-2* (Table 2, Supplementary Table 7). There were also 3 *spe* genes downregulated when both NHR-23 and SPE-44 were depleted (Table 2). The presenilin paralog SPE-4 localizes to FB-MOs and is required for cytoplasmic

partitioning during spermatogenesis (L'Hernault *et al.* 1988; Arduengo *et al.* 1998). A *spe-4* promoter reporter was used by Kulkarni *et al.* to validate their microarray data and confirm that it was not regulated by *spe-44*. The paternal effect factor SPE-11 prevents polyspermy and is required for eggshell formation (Hill *et al.* 1989), and SPE-15, a myosin VI homolog expressed in primary spermatocytes, is required for asymmetric partitioning of components such as FB-MOs and mitochondria during residual body formation (Kelleher *et al.* 2000; Hu *et al.* 2019).

Fifteen differentially regulated genes were common to NHR-23-, SPE-44-, and NHR-23+SPE-44-depleted animals (Fig. 2). Three of these genes were MFP2 paralogs (*nsph-3.2*, *nsph-4.1*, *nsph-4.2*; Table 2). MFP2 enhances MSP polymerization in *Ascaris* sperm, countering the activity of MFP1 (Grant *et al.* 2005), and there are 8 MFP2 paralog genes in *C. elegans* which have been assigned the nematode-specific peptide family, group H (*nsph*) gene class

Table 2. Differential regulation of select genes implicated in spermatogenesis.

Gene	Log2 fold change following depletion of:			Function
	NHR-23	**SPE-44**	**NHR-23+SPE-44**	
msd-1	−2.51 (1.02E−06)	—	−3.13 (1.62E−11)	MFP1 paralog. Potential role in slowing MSP polymerization
msd-2	−2.42 (6.87E−07)	—	−3.11 (1.51E−12)	MFP1 paralog. Potential role in slowing MSP polymerization
msd-3	−2.14 (4.38E−04)	—	−2.73 (1.51E−12)	MFP1 paralog. Potential role in slowing MSP polymerization
smz-1	—	—	−3.48 (6.40E−08)	Chromatin-bound protein. RNAi causes meiotic metaphase arrest.
smz-2	−5.00 (1.43E−30)	—	−5.16 (6.59E−33)	Chromatin-bound protein. RNAi causes meiotic metaphase arrest.
elt-1	—	−1.12 (4.77E−02)	−1.21 (3.78E−02)	Transcription factor that regulates msp gene expression. Regulated by spe-44 in Kulkarni et al. (2012) microarray.
msp-49	—	−1.51 (9.29E−03)	−2.57 (2.55E−08)	MSP gene. Regulated by spe-44 in Kulkarni et al. (2012) microarray.
msp-63	—	−2.17 (8.50E−06)	−1.56 (7.07E−03)	MSP gene. Regulated by spe-44 in Kulkarni et al. (2012) microarray.
spe-4	—	—	−1.74 (2.64E−02)	Required for cytoplasmic partitioning.
spe-9	—	−3.74 (2.23E−04)	−5.71 (2.96E−07)	Membrane protein required for fertilization.
spe-11	—	—	−1.23 (1.31E−02)	Prevents polyspermy and required for eggshell formation
spe-15	—	—	−2.61 (1.81E−07)	Myosin IV homolog required for cytoplasmic partitioning.
spe-18	—	−1.59 (5.97E−03)	−5.50 (8.95E−35)	Promotes MSP assembly within FBs. Regulated by spe-44 in Kulkarni et al. (2012) microarray.
spe-42	—	−2.04 (3.31E−02)	−3.35 (3.13E−05)	Membrane protein required for fertilization.
spe-43	—	−3.78 (3.67E−04)	−6.99 (1.80E−05)	Required for sperm activation.
spe-45	—	−4.44 (1.13E−06)	−4.77 (1.56E−07)	Required for spermatozoa fusion with the oocyte plasma membrane.
spe-49	—	−3.25 (7.53E−05)	−6.25 (3.48E−09)	Membrane protein required for fertilization.
nsph-1.1	—	—	−2.18 (2.90E−03)	MFP1 paralog. Potential role in promoting MSP polymerization
nsph-2	—	−1.70 (1.05E−03)	—	MFP1 paralog. Potential role in promoting MSP polymerization
nsph-3.1	—	−1.26 (3.06E−02)	−1.53 (3.59E−03)	MFP1 paralog. Potential role in promoting MSP polymerization
nsph-3.2	−1.52 (1.50E−02)	−2.26 (4.17E−07)	−4.94 (1.59E−35)	MFP1 paralog. Potential role in promoting MSP polymerization
nsph-4.1	−8.32 (3.71E−67)	−5.97 (1.16E−40)	−8.35 (9.11E−68)	MFP1 paralog. Potential role in promoting MSP polymerization
nsph-4.2	−8.55 (1.00E−72)	−6.11 (6.61E−45)	−8.57 (2.36E−73)	MFP1 paralog. Potential role in promoting MSP polymerization

(Supplementary Fig. 3; Rödelsperger et al. 2021). nsph-2 is downregulated when SPE-44 is depleted, nsph-3.1 is found in both the SPE-44 and NHR-23+SPE-44 depleted differentially regulated genes, and nsph-1.1 is downregulated only when both NHR-23 and SPE-44 are depleted (Table 2). Two nsph genes (1.2, 4.3) are not found in any of the datasets. We note that nsph-4.3 has a large deletion that removes 500 bp of sequence, though a predicted protein product can still be produced (Supplementary Figs. 3 and 4). There is also a pseudogene MFP2 paralog (ZK546.7) downregulated following NHR-23-, SPE-44, and NHR-23+SPE-44 depletion. This pseudogene is related to nsph-4.1 and nsph-4.2 but an insertion causes a frameshift. An initiation codon further downstream could produce a valid coding sequence, so this pseudogene may be worth future exploration (Supplementary Fig. 4).

NHR-23 and SPE-44 targets are enriched in phosphatase genes

To gain insight into how NHR-23 and SPE-44 promote spermatogenesis, we performed gene ontology (GO) analysis on the differentially regulated genes to identify enriched biological processes. Phosphatases were enriched in all 3 depletion conditions (Table 3, Supplementary Tables 5–7). Notably, kinase and phosphatase genes are over-represented in sperm-enriched genes (Reinke et al. 2000). The NHR-23-regulated genes were also enriched in genes involved in ATP binding, though these genes overlapped with the phosphatase genes and cytoskeletal protein binding (Supplementary Table 8). SPE-44-regulated genes were enriched in genes involved in DNA replication (origin binding, helicase activity, single-strand DNA-dependent ATPase), carbohydrate-binding, glutamate-ammonia ligase activity, and calcium ion-binding (Supplementary Table 9). In addition to being enriched in phosphatase-related GO terms, the NHR-23+SPE-44-regulated genes were also enriched in kinase genes, NADPH reductase activity, FFAT motif binding, drug binding, and transaminase activity (Supplementary Table 10). Together, these data

implicate NHR-23 and SPE-44 in regulating signal transduction by kinases and phosphatases, which has been shown to be an important regulatory mode following transcriptional quiescence in spermatocytes (Muhlrad and Ward 2002; Bae et al. 2009; Wu et al. 2012).

NHR-23 regulates uncharacterized kinases and MFP2 paralogs

We focused on the NHR-23-regulated genes as they were few in number so therefore amenable to a candidate-based knock-out approach. In addition to the aforementioned phosphatase and nsph genes, NHR-23 also regulated 4 uncharacterized kinases (Table 3). Three of these kinases were predicted to be Casein Kinase I orthologs. W03G9.5 and C04G2.2 belong to the Tau Tubulin Kinase-Like subgroup, while ZK596.2 belongs to the nematode spe-6 subgroup (Manning 2005). We engineered predicted null mutant alleles through insertion of a "STOP-IN" cassette containing premature termination codons in all 3 reading frames in the first or second exon of targeted genes (Wang et al. 2018). We generated mutants in 1 phosphatase (ZK757.2), 2 kinases (ttbk-5, ZK596.2), and 3 MFP2 paralogs (nsph-2, nsph-3.2, nsph-4.3) all of which were viable with wild-type brood sizes (Table 4). The genes nsph-4.1 and nsph-4.2 are predicted to produce identical proteins, only differ by a single nucleotide in an intron, and have 1,231 bases of identical upstream promoter sequence. This sequence similarity made genotyping a STOP-IN insertion challenging, so we deleted the entire gene for each using crRNAs that bound outside the conserved sequence for each gene. Each mutant had a wild-type brood size and no obvious increase in unfertilized oocytes (Table 4). These data could suggest that these genes are dispensable for fertility, redundant with other genes, or the STOP-IN cassette is not creating a null. We created nsph-2; nsph-1.1 and nsph-4.1, nsph-4.2 double mutants, both of which had wild-type brood sizes.

Table 3. NHR-23-regulated kinases and phosphatases.

Gene	Log2 fold-change	Class	Ortholog
ZK596.2	−9.01	Predicted serine/threonine kinase	Tau-tubulin kinase 2 (human); Casein kinase I delta ortholog
W03G9.5	−8.19	Predicted serine/threonine kinase	Casein kinase delta (human) and Casein kinase I (yeast)
F47B3.2	−4.17	Predicted tyrosine phosphatase	Tyrosine-protein phosphatase nonreceptor type 6 isoform 3 (mammals)
F55H12.5	−4.04	Predicted tyrosine phosphatase	Receptor-type tyrosine-protein phosphatase T (mammals)
F47B3.7	−4	Predicted tyrosine phosphatase	Tyrosine-protein phosphatase nonreceptor type 6 isoform 3 (mammals)
ZK757.2	−3.49	Predicted tyrosine/serine/threonine phosphatase	Dual specificity phosphatase 14 (human)
D2045.7	−3.05	Predicted serine/threonine kinase	Serine/threonine kinase 16 (human)
F52H3.6	−2.7	Predicted serine/threonine phosphatase	Isoform Gamma-1 of Serine/threonine-protein phosphatase PP1-gamma catalytic subunit (humans)
ttbk-5	−2.01	Predicted serine/threonine kinase	Tau-tubulin kinase 2 (human); Casein kinase I delta ortholog

Table 4. Brood size data.

Genotype	Allele class	Predicted gene function	Brood size ($\pm$SD)	% unfertilized eggs
N2 (wt)	N/A	N/A	230 $\pm$ 91	3.2 ($n = 2{,}891$)
nsph-2(wrd57)	PTC	MFP2 paralog	301 $\pm$ 43	2.75 ($n = 2{,}184$)
nsph-3.2(wrd56])	PTC	MFP2 paralog	277 $\pm$ 39	2.34 ($n = 3{,}420$)
nsph-2(wrd57); nsph-3.2(wrd56)	PTC	MFP2 paralog	293 $\pm$ 39	1.5 ($n = 3{,}276$)
nsph-2(wrd57); nsph-1.1(wrd67)	PTC	MFP2 paralog	185 $\pm$ 40	1.07 ($n = 2{,}241$)
nsph-4.3(wrd74)	PTC	MFP2 paralog	277 $\pm$ 49	3.08 ($n = 3{,}445$)
nsph-4.1(wrd92)	Whole gene deletion	MFP2 paralog	228 $\pm$ 45	5.75 ($n = 2{,}677$)
nsph-4.2(wrd93)	Whole gene deletion	MFP2 paralog	219 $\pm$ 35	4.15 ($n = 2{,}750$)
nsph-4.1(wrd92), nsph-4.2(wrd97)	Whole gene deletion	MFP2 paralog	260 $\pm$ 49	4.64 ($n = 3{,}296$)
ttbk-5(wrd72)	PTC	Kinase	259 $\pm$ 25	6.84 ($n = 3{,}373$)
ZK596.2(wrd71)	PTC	Kinase	231 $\pm$ 80	2.93 ($n = 2{,}931$)
ZK757.2(wrd77)	PTC	Phosphatase	242 $\pm$ 17	3.31 ($n = 2{,}999$)

NHR-23-depletion causes NSPH-2 and MSD-1 localization defects

As previously described, both NSPH-2 and MSD-1 antibodies label FBs and colocalize with MSP antibody labeling in wild-type 1° spermatocytes (Morrison *et al.* 2021; Fig. 3, a and b). In other studies (Kulkarni *et al.* 2012; Ragle *et al.* 2020), we found that single and double NHR-23 and SPE-44 germline depletion have distinct effects on FB-MO formation. Single depletions of either NHR-23 or SPE-44 fully disrupt the assembly of MSP into FBs but differentially impact the MO component of the FB-MO complex (Kulkarni *et al.* 2012; Ragle *et al.* 2020). When labeled with the MO differentiation marker 1CB4, NHR-23 depleted spermatocytes exhibit distinct labeled structures, whereas 1CB4 labeling is diffuse in SPE-44 depleted spermatocytes and absent in the NHR-23+SPE-44 depleted spermatocytes (Ragle *et al.* 2020). To further explore these interactions, we tested how depleting NHR-23, SPE-44, and NHR-23+SPE-44 from the germline would affect the localization of other FB components such as NSPH-2 and MSD-1. In each of our depletion strains, germline labeling with anti-NSPH-2 and anti-MSD-1 was dim and diffuse, compared to the bright puncta labeled in control germlines, indicating that assembly of NSPH-2 and MSD-1 into FBs was impaired in the absence of NHR-23, SPE-44, or both. Although our RNA-seq data suggest that SPE-44 and not NHR-23 regulates *nsph-2* (Table 2), terminal SPE-44 depleted spermatocytes exhibited NSPH-2 aggregates that were not observed in either NHR-23 or the double-depleted strains (Fig. 3a). Due to this unexpected phenotype, we also investigated *spe-44* null (*ok1400*) mutants (Kulkarni *et al.* 2012). Auxin-inducible depletion of target proteins is robust, but may not be fully penetrant in some cases, so the null mutant provides additional insight into *spe-44*'s role in FB assembly. Consistent with our RNA-seq results, anti-NSPH did not label germlines in *spe-44(ok1400)* animals

(Fig. 3a'). As predicted from our RNA-seq data (Table 2), antibody labeling with anti-MSD-1, which labels all MSD isoforms (Kosinski *et al.* 2005), was most diminished in NHR-23 and NHR-23+SPE-44 depleted spermatocytes, whereas terminal SPE-44 depleted spermatocytes exhibited dim but detectable MSD-1 punctae (Fig. 3b). In both single and double depletions, the MSD-1 antibody labeled centrosomes (arrows), but the significance of this pattern is unclear (Fig. 3b). It may be nonspecific as many preimmune sera label the centrosomes of nematode spermatocytes. Alternatively, in the absence of normal FBs, perhaps centrosomes serve as a secondary localization site for the remaining MSD-1 protein. These data indicate that NHR-23 is either required for the stable expression of NSPH-2 and MSD-1 or for localization of NSPH-2 and MSD-1 to the FB-MO complex, which is consistent with our previous finding that NHR-23 depletion prevents MSP loading into FBs (Ragle *et al.* 2020).

SPE-6 patterns are differentially affected in single and double knockdowns

Given our finding that NHR-23 regulates 3 uncharacterized Casein Kinase I orthologs, W03G9.5, C04G2.2, and ZK596.2, which belong to the nematode *spe-6* subgroup, we decided to investigate the localization of SPE-6, the better characterized casein kinase 1 ortholog, in our depletion strains. In *C. elegans*, *spe-6* encodes one of a large family of casein kinase 1 proteins (Muhlrad and Ward 2002). Like NHR-23 and SPE-44 depletion, SPE-6 null mutations result in primary spermatocyte arrest (Varkey *et al.* 1993). During wild-type spermatogenesis, SPE-6 shifts from a diffuse plus particulate pattern in spermatocytes to being localized around the condensed haploid chromatin mass during the budding division that follows anaphase II (Peterson *et al.* 2021; Fig. 4a). Although *spe-6* transcript levels were not significantly altered in either the
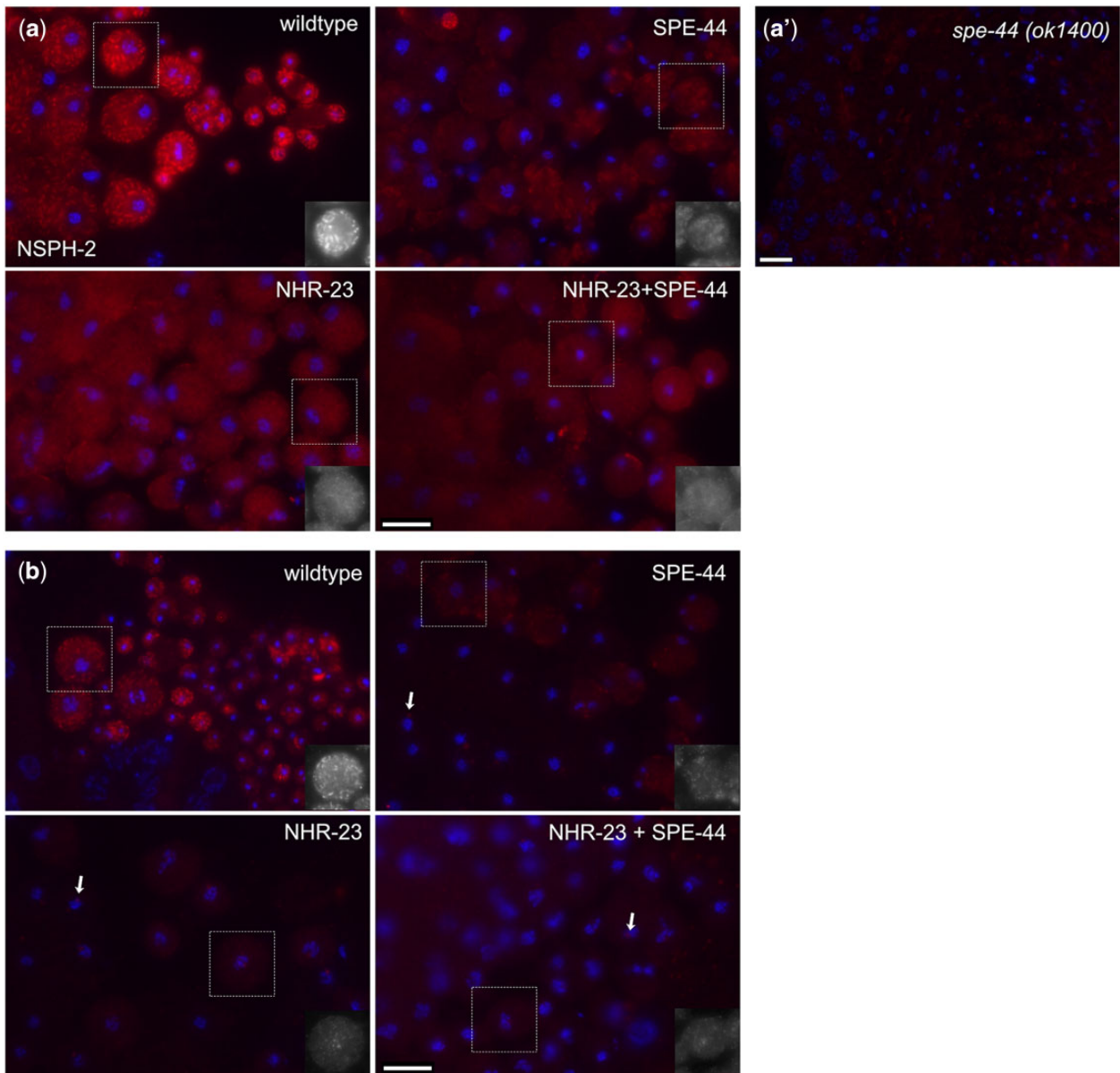
Fig. 3. NSPH-2 and MSD-1 in NHR-23, SPE-44, and NHR-23+SPE-44 depleted spermatocytes. Monolayer of isolated spermatocytes; and, in wild type, budding figures and spermatids labeled with DAPI (blue) and either anti-NSPH-2 antibody (a) or anti-MSD-1 antibody (b) (red). Images are oriented with earlier stages on the left. In the images shown, wild-type spermatocytes are from JDW92 males that contain the *nhr-23* degron constructs but were not auxin-treated (a, b). The other images are from males in which the indicated transcription factor has been depleted by auxin-mediated degradation. Images are representative of multiple preparations, but images shown are from the same preparation and taken with the same exposures without additional adjustments. a') Monolayer of isolated spermatocytes from *spe-44(ok1400)* null mutant labeled with anti-NSPH-2 antibody. b) Arrows show labeled centrosomes. In a and b, black and white inserts of indicated spermatocytes are shown for clarity. Scale bars = 10 μm.

single or double depletion strains (Supplementary Table 1), we tested whether either the SPE-6 localization patterns or levels of abundance would be differentially altered when we used anti-SPE-6 antibody to label the proximal germlines of affected males. In NHR-23 depleted spermatocytes, SPE-6 remains in a diffuse plus particulate pattern, consistent with its early meiosis I arrest (Fig. 4b). In contrast, in SPE-44 depleted spermatocytes, SPE-6 clumps around the chromatin masses in a postmeiotic-like pattern even though the spermatocytes never physically divide to form haploid spermatids (Fig. 4c, Kulkarni *et al.* 2012). Anti-SPE-6 labeling in NHR-23+SPE-44 depleted germlines exhibited 2 distinct phenotypes: most (51/67) were similar to the NHR-23 single depletion but with overall reduced levels and cell-to-cell variability (Fig. 4d) whereas others (16/67) failed to label with SPE-6

antibodies (Fig. 4e). These data suggest that the developmental program of restructuring the sperm chromatin continues upon SPE-44 depletion but not upon NHR-23 depletion, and that SPE-6 expression is reduced or lost upon NHR-23+SPE-44-depletion.

Discussion

This work identifies genes differentially regulated following NHR-23-depletion in male germlines, providing insight into how NHR-23 promotes spermatogenesis. We also identify genes that are differentially expressed only when both NHR-23 and SPE-44 are depleted in male germlines. This list provides an entry point to understanding the synthetic phenotype associated with depleting both transcription factors (Ragle *et al.* 2020). NHR-23 depletion
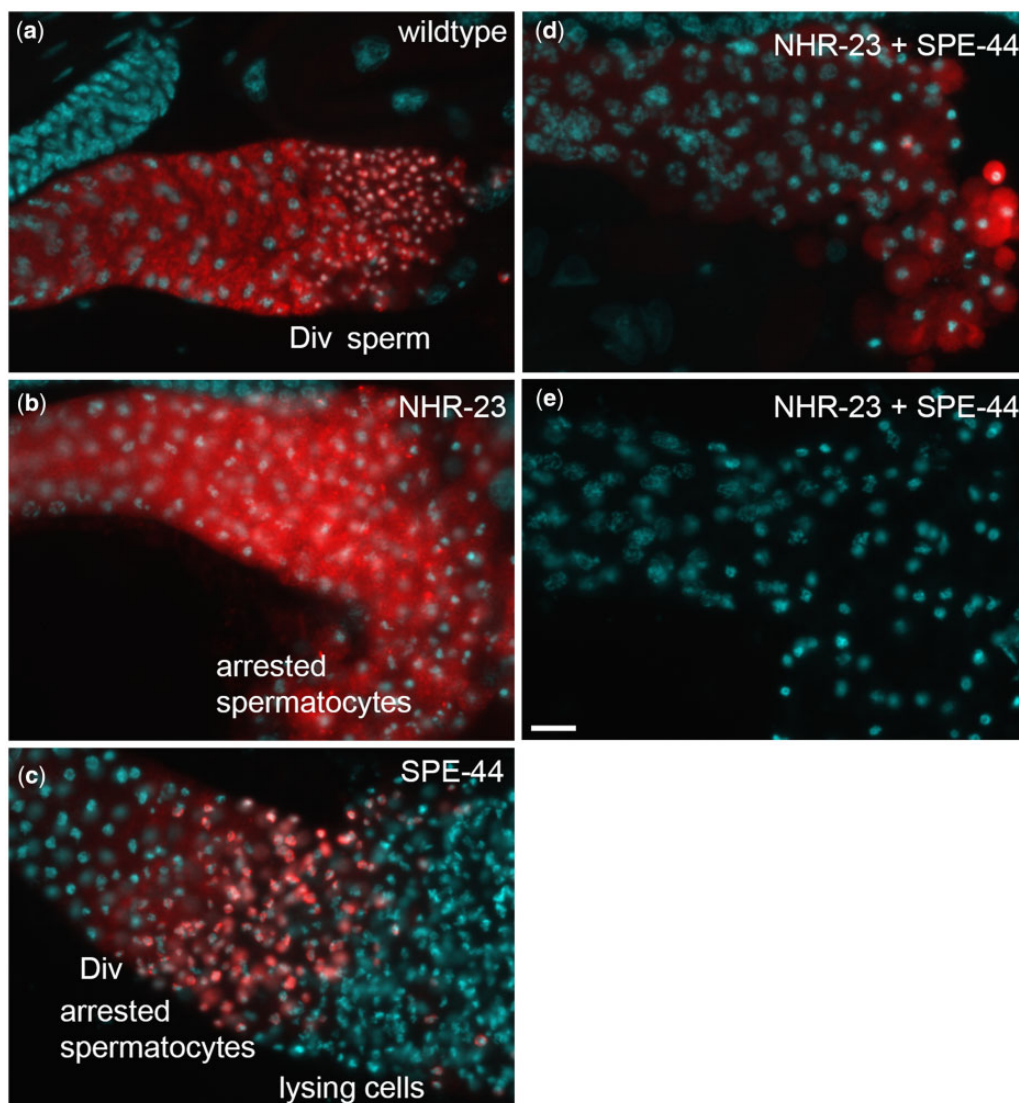
Fig. 4. SPE-6 patterns in NHR-23, SPE-44, and NHR-23+SPE-44 depleted spermatocytes. Proximal regions of male gonads labeled with DAPI (cyan) and anti-SPE-6 antibody (red). Images are oriented with earlier stages on the left. a) Wild-type controls are auxin-treated *him*-5 males. b–e) The other images are from males in which the indicated transcription factor has been depleted by auxin-mediated degradation. The regions of the gonad are labeled including the meiotic division zone (DIV). Images are representative of multiple preparations, but images shown are from the same preparation and taken with the same exposures without additional adjustments. Scale bars = 10 μm.

causes defective localization of NSPH-2 and MSD-1 to FBs, implicating NHR-23 in regulating MSP polymerization dynamics. Although NHR-23 and SPE-44 do not appear to transcriptionally regulate the Casein kinase *spe*-6, double depletion of these transcription factors causes a partial or severe loss of SPE-6 antibody labeling, suggesting that SPE-6 protein levels are compromised when NHR-23 and SPE-44 are absent from the germline.

NHR-23 regulates few genes with known roles in spermatogenesis

Relatively few genes were differentially regulated following NHR-23-depletion (Supplementary Table 5; 70 genes) compared to SPE-44-depletion (Supplementary Table 6; 811 genes), NHR-23+SPE-44-depletion (Supplementary Table 7; 554 genes), or *nhr-23(RNAi)* in L2 larvae (Kouns *et al.* 2011). Aside from *smz-2*, none of the NHR-23-regulated genes have been experimentally confirmed to play roles in spermatogenesis.

Terminally arrested spermatocytes from NHR-23 depleted animals arrest early in meiosis and contain distended MOs, similar

to *spe-6(lf)* and *wee-1.3(gf)* mutants (Varkey *et al.* 1993; Lamitina and L'Hernault 2002), yet NHR-23 does not regulate these genes (Supplementary Tables 1 and 5). The dearth of known spermatogenesis regulators is consistent with NHR-23 regulating a novel pathway promoting sperm development. As NHR-23 regulates several uncharacterized kinases and phosphatases, one possibility is that NHR-23 controls meiotic progression and FB-MO biogenesis through kinase-mediated signal transduction. The orthologs of 2 of the kinases identified in our RNA-seq dataset (*ttbk-5, ZK596.2*) are implicated in mammalian microtubule dynamics and yeast vesicular traffic, meiotic exit, and kinetochore attachment in meiosis II (Petronczki *et al.* 2006; Goetz *et al.* 2012; Lee *et al.* 2017). While our STOP-IN insertions did not have phenotypes, there could be redundancy or genetic compensation, a point which we will expand on in the next section.

NHR-23 is necessary for MSD-1 and NSPH-2 localization

Our immunostaining revealed that NHR-23 depletion caused a loss of MSD-1 and NSPH-2 localization in spermatocytes. The orthologs of these factors (MFP1 and MFP2) in *Ascaris* are specifically known to control MSP polymerization within the pseudopod of crawling sperm (Buttery *et al.* 2003; Grant *et al.* 2005) but since they are also present in FBs (Morrison *et al.* 2021), their downregulation upon NHR-23 depletion might account for the observed defect in MSP loading into FB-MOs (Ragle *et al.* 2020). The effect of NHR-23 on NSPH-2 localization was surprising as this gene was not differentially regulated following NHR-23 depletion (Table 1, Supplementary Table 5). *nsph-2* was downregulated following SPE-44 depletion (Table 1, Supplementary Table 5); and by immunocytology, the protein expression appeared slightly reduced in SPE-44-depleted germlines and significantly reduced in *spe-44(ok1400)* null mutants (Fig. 3). These data suggest that NHR-23 could promote NSPH localization to FB-MOs. There are 4 uncharacterized MSD1 paralogs in *C. elegans*, all of which are recognized by the MSD-1 antibody and 3 of which are regulated by NHR-23 (Table 1, Supplementary Table 5). There are 8 MFP2 paralogs, which are also uncharacterized. Three of these paralogs are regulated by NHR-23 while 5 are SPE-44-regulated (Table 2). No phenotype has been previously reported for the *C. elegans* MFP1 or MFP2 paralogs, though redundancy may be responsible since these paralogs appear to have arisen through duplication. We have inactivated 6 of the MFP2 paralogs either singly or in double mutant combinations and have seen no difference in fertility. Three possible explanations for the lack of phenotype are: (1) that these genes do not play a role in *C. elegans* spermatogenesis; (2) extensive genetic redundancy exists and we will have to inactivate more paralogs, if not all, to produce a phenotype; or (3) that our knock-out approach caused genetic compensation, where mRNAs containing premature stop codons trigger the upregulation of paralogous genes (Rossi *et al.* 2015; El-Brolosy *et al.* 2019). We favor the second and third possibilities. Going forward, it will be important to avoid genetic compensation by systematically deleting MFP1 and MFP2 orthologs or use a multiplexed piRNA-based knockdown approach to determine whether these genes play roles in *C. elegans* MSP polymerization dynamics (Priyadarshini *et al.* 2022).

A high-confidence set of *spe-44*-regulated genes

There was a surprising lack of overlap between the SPE-44-regulated genes in our RNA-seq dataset and differentially regulated genes in a *spe-44* mutant microarray dataset (Kulkarni *et al.* 2012), though the genes common to both datasets are high-confidence *spe-44* targets. The difference could be biological as the *spe-44* mutant is a predicted null, while auxin-mediated protein depletion frequently produces hypomorphic phenotypes as we also observed in our NSPH-2 immunocytology. Our data were generated from adult males, while the *spe-44* mutant dataset was generated from L4 males, so it is also possible that differences in developmental stage impacted the results. While RNA-seq is reported to have a wider quantitative range in detecting changes in expression levels, a comparison of microarrays vs RNA-seq on rat cDNA reported a 78% overlap in differentially regulated genes (Rao *et al.* 2019). The genes common to both datasets include *elt-1*, a transcription factor that acts downstream of SPE-44 to regulate MSP gene expression, and *ceh-48* (del Castillo-Olivares *et al.* 2009; Kulkarni *et al.* 2012). *ceh-48* is an uncharacterized ONECUT homeobox transcription factor ortholog that Kulkarni *et al.* (2012)

identified as sperm-enriched. A deletion mutant is reported to be fertile but displays male tail defects (Kim *et al.* 2016). *spe-18*, which promotes MSP assembly within FBs, and the MFP2 paralog *nsph-2* were also common to both datasets (Price *et al.* 2021). Exploring the high confidence target will provide insight into how SPE-44 promotes FB-MO assembly and meiosis II.

SPE-6 labeling is reduced or lost in NHR-23+ SPE-44 depleted germlines

SPE-6 is a casein kinase that plays broad roles in spermatogenesis including FB assembly, meiotic progression, and repression of precocious sperm activation (Varkey *et al.* 1993; Muhlrad and Ward 2002; Peterson *et al.* 2021; Price *et al.* 2021). *spe-6* was not differentially regulated in any of our datasets, despite the overlap of the NHR-23-depletion and *spe-6(lf)* meiotic arrest and distended FB-MO phenotype (Varkey *et al.* 1993; Ragle *et al.* 2020). SPE-6 labeling in NHR-23-depleted animals appeared in a punctate pattern, as well as diffuse in the cytosol, as expected in metaphase I arrested spermatocytes (Ragle *et al.* 2020; Fig. 4c). In SPE-44-depleted germlines, SPE-6 labeling appeared similar to a postmeiotic pattern, despite the meiosis II arrest and lack of spermatocytes (Kulkarni *et al.* 2012; Fig. 4b). These data suggest that progression through metaphase I is required for SPE-6 to localize around chromatin after meiosis, and that this localization and presumably SPE-6 pathway is insensitive to SPE-44 depletion and the meiosis II arrest. Surprisingly, NHR-23+SPE-44 double-depletion caused a partial or complete loss of SPE-6 labeling, another example of a synthetic phenotype caused by depletion of these transcription factors (Fig. 4, d and e). *spe-6* transcript levels were not significantly affected by NHR-23+SPE-44 depletion (Supplementary Table 1), indicating that this SPE-6 downregulation is not transcriptional. Possible mechanisms could include impaired translation of *spe-6* mRNA or an increase in SPE-6 turnover.

Future perspectives

We previously discovered a novel role for NHR-23 in spermatogenesis and a synthetic interaction between NHR-23 and SPE-44 (Ragle *et al.* 2020). We also proposed that a yet-undetermined pathway promoted spermatogenesis independently of NHR-23 and SPE-44 (Ragle *et al.* 2020). In agreement with this assertion, there are a large number of sperm-enriched genes not found in our differentially regulated gene lists, and there are genes only differentially regulated following NHR-23+SPE-44 depletion, consistent with synthetic interaction. Numerous experimentally validated *spe* genes are not regulated by NHR-23 or SPE-44. Our RNA-seq data provide an entry point to understanding transcriptional control of *C. elegans* spermatogenesis and how NHR-23 and SPE-44 interact to promote FB-MO biogenesis.

Data availability

The data underlying this article are available in the article and in its online supplementary material. Strains and plasmids are available upon request. Supplementary File 1 contains the genomic sequence of wild-type and genome-edited loci. The RNA-seq data have been deposited in the National Center for Biotechnology Information Gene Expression Omnibus under accession number GSE206676. Supplementary Table 1 contains the processed data with gene name and location, mean expression, log2 fold-change compared to control, and *P*-value. Sequences and descriptions of the crRNAs and repair oligos are provided in Supplementary Tables 2 and 3, respectively. Genotyping primers are provided in Supplementary Table 4.

Supplemental material is available at G3 online.

Funding

Conflicts of interest

None declared.

Literature cited

Anders S, Pyl PT, Huber W. HTSeq—a Python framework to work with high-throughput sequencing data. Bioinformatics. 2015; 31(2):166–169.

Arduengo PM, Appleberry OK, Chuang P, L'Hernault SW. The presenilin protein family member SPE-4 localizes to an ER/Golgi derived organelle and is required for proper cytoplasmic partitioning during *Caenorhabditis elegans* spermatogenesis. J Cell Sci. 1998;111(24):3645–3654.

Ashley GE, Duong T, Levenson MT, Martinez MAQ, Johnson LC, Hibshman JD, Saeger HN, Palmisano NJ, Doonan R, Martinez-Mendez R, *et al.* An expanded auxin-inducible degron toolkit for *Caenorhabditis elegans*. Genetics. 2021;217(3):iyab006.

Bae Y-K, Kim E, L'hernault SW, Barr MM. The CIL-1 PI 5-phosphatase localizes TRP polycystins to cilia and activates sperm in *C. elegans*. Curr Biol. 2009;19(19):1599–1607.

Bettegowda A, Wilkinson MF. Transcription and post-transcriptional regulation of spermatogenesis. Philos Trans R Soc Lond B Biol Sci. 2010;365(1546):1637–1651.

Brenner S. The genetics of *Caenorhabditis elegans*. Genetics. 1974; 77(1):71–94.

Buttery SM, Ekman GC, Seavy M, Stewart M, Roberts TM. Dissection of the *Ascaris* sperm motility machinery identifies key proteins involved in major sperm protein-based amoeboid locomotion. Mol Biol Cell. 2003;14(12):5082–5088.

Chu DS, Liu H, Nix P, Wu TF, Ralston EJ, Yates JR, Meyer BJ. Sperm chromatin proteomics identifies evolutionarily conserved fertility factors. Nature. 2006;443(7107):101–105.

Chu DS, Shakes DC. Germ cell development in *C. elegans*. In: T Schedl, editor. Advances in Experimental Medicine and Biology. New York (NY): Springer; 2013. p. 171–203.

Church DL, Guan KL, Lambie EJ. Three genes of the MAP kinase cascade, *mek-2*, *mpk-1/sur-1* and *let-60 ras*, are required for meiotic cell cycle progression in *Caenorhabditis elegans*. Development. 1995;121(8):2525–2535.

del Castillo-Olivares A, Kulkarni M, Smith HE. Regulation of sperm gene expression by the GATA factor ELT-1. Dev Biol. 2009;333(2): 397–408.

D'Occhio MJ, Hengstberger KJ, Johnston SD. Biology of sperm chromatin structure and relationship to male fertility and embryonic survival. Anim Reprod Sci. 2007;101(1–2):1–17.

Dokshin GA, Ghanta KS, Piscopo KM, Mello CC. Robust genome editing with short single-stranded and long, partially single-stranded DNA donors in *Caenorhabditis elegans*. Genetics. 2018;210(3): 781–787.

Edgar LG. Blastomere culture and analysis. Methods Cell Biol. 1995;48:303–321.

El Mouridi S, Peng Y, Frøkjær-Jensen C. Characterizing a strong pan-muscular promoter (P*mlc-1*) as a fluorescent co-injection marker to select for single-copy insertions. MicroPubl Biol. 2020;2020. doi: 10.17912/micropub.biology.000302.

El-Brolosy MA, Kontarakis Z, Rossi A, Kuenne C, Günther S, Fukuda N, Kikhi K, Boezio GLM, Takacs CM, Lai S-L, *et al.* Genetic compensation triggered by mutant mRNA degradation. Nature. 2019; 568(7751):193–197.

Ellis RE, Stanfield GM. The regulation of spermatogenesis and sperm function in nematodes. Semin Cell Dev Biol. 2014;29:17–30.

Fabian L, Brill JA. *Drosophila* spermiogenesis: big things come from little packages. Spermatogenesis. 2012;2(3):197–212.

Farboud B, Meyer BJ. Dramatic enhancement of genome editing by CRISPR/Cas9 through improved guide RNA design. Genetics. 2015;199(4):959–971.

Ghanta KS, Mello CC. Melting dsDNA Donor Molecules Greatly Improves Precision Genome Editing in Caenorhabditis elegans. Genetics. 2020;216(3):643–650.

Goetz SC, Liem KF, Anderson KV. The spinocerebellar ataxia-associated gene Tau tubulin kinase 2 controls the initiation of ciliogenesis. Cell. 2012;151(4):847–858.

Goujon M, McWilliam H, Li W, Valentin F, Squizzato S, Paern J, Lopez R. A new bioinformatics analysis tools framework at EMBL–EBI. Nucleic Acids Res. 2010;38(Web Server issue):W695–W699.

Grant RP, Buttery SM, Ekman GC, Roberts TM, Stewart M. Structure of MFP2 and its function in enhancing MSP polymerization in *Ascaris* sperm amoeboid motility. J Mol Biol. 2005;347(3):583–595.

Griswold MD. Spermatogenesis: the commitment to meiosis. Physiol Rev. 2016;96(1):1–17.

Hill DP, Shakes DC, Ward S, Strome S. A sperm-supplied product essential for initiation of normal embryogenesis in *Caenorhabditis elegans* is encoded by the paternal-effect embryonic-lethal gene, *spe-11*. Dev Biol. 1989;136(1):154–166.

Hu J, Cheng S, Wang H, Li X, Liu S, Wu M, Liu Y, Wang X. Distinct roles of two myosins in *C. elegans* spermatid differentiation. PLoS Biol. 2019;17(4):e3000211-31.

Kelleher JF, Mandell MA, Moulder G, Hill KL, L'Hernault SW, Barstead R, Titus MA. Myosin VI is required for asymmetric segregation of cellular components during *C. elegans* spermatogenesis. Curr Biol. 2000;10(23):1489–1496.

Kim B, Suo B, Emmons SW. Gene function prediction based on developmental transcriptomes of the two sexes in *C. elegans*. Cell Rep. 2016;17(3):917–928.

Kim D, Pertea G, Trapnell C, Pimentel H, Kelley R, Salzberg SL. TopHat2: accurate alignment of transcriptomes in the presence of insertions, deletions and gene fusions. Genome Biol. 2013; 14(4):R36.

Kosinski M, McDonald K, Schwartz J, Yamamoto I, Greenstein D. *C. elegans* sperm bud vesicles to deliver a meiotic maturation signal to distant oocytes. Development. 2005;132(15):3357–3369.

Kouns NA, Nakielna J, Behensky F, Krause MW, Kostrouch Z, Kostrouchova M. NHR-23 dependent collagen and hedgehog-related genes required for molting. Biochem Biophys Res Commun. 2011;413(4):515–520.

Krauchunas AR, Mendez E, Ni JZ, Druzhinina M, Mulia A, Parry J, Gu SG, Stanfield GM, Singson A. *spe-43* is required for sperm activation in *C. elegans*. Dev Biol. 2018;436(2):75–83.

Kroft TL, Gleason EJ, L'Hernault SW. The *spe-42* gene is required for sperm-egg interactions during *C. elegans* fertilization and encodes a sperm-specific transmembrane protein. Dev Biol. 2005;286(1): 169–181.

Kulkarni M, Shakes DC, Guevel K, Smith HE. SPE-44 implements sperm cell fate. PLoS Genet. 2012;8(4):e1002678.

Lamitina ST, L'Hernault SW. Dominant mutations in the *Caenorhabditis elegans* Myt1 ortholog *wee-1.3* reveal a novel domain that controls M-phase entry during spermatogenesis. Development. 2002;129(21):5009–5018.

Lee M-S, Joo JH, Kim K. Roles of budding yeast Hrr25 in recombination and sporulation. J Microbiol Biotechnol. 2017;27(6):1198–1203.

L'Hernault SW, Shakes DC, Ward S. Developmental genetics of chromosome I spermatogenesis-defective mutants in the nematode *Caenorhabditis elegans*. Genetics. 1988;120(2):435–452.

Love MI, Huber W, Anders S. Moderated estimation of fold change and dispersion for RNA-seq data with DESeq2. Genome Biol. 2014;15(12):550.

Manning G. Genomic overview of protein kinases. WormBook. 2005. doi: 10.1895/wormbook.1.60.1.

Morrison KN, Uyehara CM, Ragle JM, Ward JD, Shakes DC. MFP1/MSD-1 and MFP2/NSPH-2 co-localize with MSP during *C. elegans* spermatogenesis. MicroPublication Biol. 2021. doi:10.17912/micropub.biology.000427.

Muhlrad PJ, Ward S. Spermiogenesis initiation in *Caenorhabditis elegans* involves a casein kinase 1 encoded by the *spe-6* gene. Genetics. 2002;161(1):143–155.

Nishimura H, L'Hernault SW. Spermatogenesis. Curr Biol. 2017;27(18):R988–R994.

Nishimura H, Tajima T, Comstra HS, Gleason EJ, L'Hernault SW. The immunoglobulin-like gene *spe-45* acts during fertilization in *Caenorhabditis elegans* like the mouse *Izumo1* gene. Curr Biol. 2015;25(24):3225–3231.

Ortiz MA, Noble D, Sorokin EP, Kimble J. A new dataset of spermatogenic vs. oogenic transcriptomes in the nematode *Caenorhabditis elegans*. G3 (Bethesda). 2014;4(9):1765–1772.

Paix A, Folkmann A, Rasoloson D, Seydoux G. High efficiency, homology-directed genome editing in *Caenorhabditis elegans* using CRISPR-Cas9 ribonucleoprotein complexes. Genetics. 2015;201(1):47–54.

Peterson JJ, Tocheny CE, Prajapati G, LaMunyon CW, Shakes DC. Subcellular patterns of SPE-6 localization reveal unexpected complexities in *Caenorhabditis elegans* sperm activation and sperm function. G3 (Bethesda). 2021;11:jkab288.

Petronczki M, Matos J, Mori S, Gregan J, Bogdanova A, Schwickart M, Mechtler K, Shirahige K, Zachariae W, Nasmyth K. Monopolar attachment of sister kinetochores at meiosis I requires casein kinase 1. Cell. 2006;126(6):1049–1064.

Price KL, Presler M, Uyehara CM, Shakes DC. The intrinsically disordered protein SPE-18 promotes localized assembly of MSP in *Caenorhabditis elegans* spermatocytes. Development. 2021;148(5):dev195875.

Priyadarshini M, Ni JZ, Vargas-Velazquez AM, Gu SG, Frøkjær-Jensen C. Reprogramming the piRNA pathway for multiplexed and transgenerational gene silencing in *C. elegans*. Nat Methods. 2022;19(2):187–194.

R Core Team. R: A Language and Environment for Statistical Computing. Vienna (Austria): R Foundation for Statistical Computing. https://www.R-project.org/

Ragle JM, Aita AL, Morrison KN, Martinez-Mendez R, Saeger HN, Ashley GA, Johnson LC, Schubert KA, Shakes DC, Ward JD. The conserved molting/circadian rhythm regulator NHR-23/NR1F1 serves as an essential co-regulator of *C. elegans* spermatogenesis. Development. 2020;147:dev193862.

Rao MS, Van Vleet TR, Ciurlionis R, Buck WR, Mittelstadt SW, Blomme EAG, Liguori MJ. Comparison of RNA-Seq and microarray gene expression platforms for the toxicogenomic evaluation of liver from short-term rat toxicity studies. Front Genet. 2019;9:636.

Rathke C, Baarends WM, Jayaramaiah-Raja S, Bartkuhn M, Renkawitz R, Renkawitz-Pohl R. Transition from a nucleosome-based to a protamine-based chromatin configuration during spermiogenesis in *Drosophila*. J Cell Sci. 2007;120(Pt 9):1689–1700.

Reinke V, Smith HE, Nance J, Wang J, Van Doren C, Begley R, Jones SJ, Davis EB, Scherer S, Ward S, *et al.* A global profile of germline gene expression in *C. elegans*. Mol Cell. 2000;6(3):605–616.

Rödelsperger C, Ebbing A, Sharma DR, Okumura M, Sommer RJ, Korswagen HC. Spatial transcriptomics of nematodes identifies sperm cells as a source of genomic novelty and rapid evolution. Mol Biol Evol. 2021;38(1):229–243.

Rossi A, Kontarakis Z, Gerri C, Nolte H, Hölper S, Krüger M, Stainier DYR. Genetic compensation induced by deleterious mutations but not gene knockdowns. Nature. 2015;524(7564):230–233.

Shakes DC, Wu J-C, Sadler PL, Laprade K, Moore LL, Noritake A, Chu DS. Spermatogenesis-specific features of the meiotic program in *Caenorhabditis elegans*. PLoS Genet. 2009;5(8):e1000611.

Sievers F, Wilm A, Dineen D, Gibson TJ, Karplus K, Li W, Lopez R, McWilliam H, Remmert M, Söding J, *et al.* Fast, scalable generation of high-quality protein multiple sequence alignments using Clustal Omega. Mol Syst Biol. 2011;7:539.

Singson A, Mercer KB, L'Hernault SW. The *C. elegans spe-9* gene encodes a sperm transmembrane protein that contains EGF-like repeats and is required for fertilization. Cell. 1998;93(1):71–79.

Smith HE. Nematode sperm motility. WormBook. 2014;1–15. doi: 10.1895/wormbook.1.68.2.

Takayama J, Tajima T, Onami S, Nishimura H. *C. elegans* spermatozoa lacking *spe-45* are incapable of fusing with the oocyte plasma membrane. MicroPubl Biol. 2021;2021. doi: 10.17912/micropub.biology.000372.

Varkey JP, Jansma PL, Minniti AN, Ward S. The *Caenorhabditis elegans spe-6* gene is required for major sperm protein assembly and shows second site non-complementation with an unlinked deficiency. Genetics. 1993;133(1):79–86.

Wang H, Park H, Liu J, Sternberg PW. An efficient genome editing strategy to generate putative null mutants in *Caenorhabditis elegans* using CRISPR/Cas9. G3 (Bethesda). 2018;8(11):3607–3616.

Waterhouse AM, Procter JB, Martin DMA, Clamp M, Barton GJ. Jalview Version 2—a multiple sequence alignment editor and analysis workbench. Bioinformatics. 2009;25(9):1189–1191.

Wilson LD, Obakpolor OA, Jones AM, Richie AL, Mieczkowski BD, Fall GT, Hall RW, Rumbley JN, Kroft TL. The *Caenorhabditis elegans spe-49* gene is required for fertilization and encodes a sperm-specific transmembrane protein homologous to SPE-42. Mol Reprod Dev. 2018;85(7):563–578.

Wu J-C, Go AC, Samson M, Cintra T, Mirsoian S, Wu TF, Jow MM, Routman EJ, Chu DS. Sperm development and motility are regulated by PP1 phosphatases in *Caenorhabditis elegans*. Genetics. 2012;190(1):143–157.

Wu TF, Chu DS. Sperm chromatin. Mol Cell Proteomics. 2008;7(10):1876–1886.

Zannoni S, L'Hernault SW, Singson AW. Dynamic localization of SPE-9 in sperm: a protein required for sperm-oocyte interactions in *Caenorhabditis elegans*. BMC Dev Biol. 2003;3:10.